Enhanced electrical and thermoelectric properties from textured $Bi_{1.6}Pb_{0.4}Ba_2Co_2O_y$/Ag composites

M. A. Madre[1], Sh. Rasekh[1], M. A. Torres[1], P. Bosque[2], J. C. Diez[1], A. Sotelo[1,*]

[1]ICMA (CSIC-Universidad de Zaragoza), Dpt. Ciencia de Materiales, 50018-Zaragoza, Spain.

[2]Universidad de Zaragoza, Dpt. Expresion Grafica en la Ingenieria, 50018-Zaragoza, Spain.

Abstract

$Bi_{1.6}Pb_{0.4}Ba_2Co_2O_y$/3 wt. %Ag composites have been textured using the laser floating zone technique. Microstructural observations have shown the formation of a relatively high amount of secondary phases and cracks along the plate-like grains in the as-grown materials. In spite of these microstructural features, electrical properties have not been drastically decreased. Annealing of these as-grown rods has enhanced the grains connectivity, decreased the secondary phases content, and healed the cracks, increasing their electrical performances. It has been deduces that oxygen content in the thermoelectric phase has not been significantly modified through annealing, as demostrated by the very similar Seebeck values at room temperature in the as-grown and annealed samples. As a consequence of the low electrical resistivity values in the annealed materials, they reached higher power factor values than the as-grown ones. The highest power factor at room temperature is in the range of the reported for single crystals, while at 650 ºC it is the highest reported in Bi-Ba-Co-O polycrystalline family so far.

Keywords: Ceramic composites; Oxides; Grain growth; Electrical resistivity; Power factor

* asotelo@unizar.es
Tel.: +34 976762617
Fax: +34 976761957

Acknowledgements

This research has been supported by the MINECO-FEDER (Project MAT2013-46505-C3-1-R). The authors wish to thank the Gobierno de Aragón-FEDER (Consolidated Research Groups T87 and T12) for financial support. Authors acknowledge the use of Servicio General de Apoyo a la Investigación-SAI, Universidad de Zaragoza.

Introduction

Thermoelectric (TE) power generation is a promising technology to harvest wasted heat from different energy transforming systems. As a consequence, it can raise the efficiency of these systems, reducing CO_2 emissions and fighting against global warming. For these practical applications it is necessary to produce high efficiency TE materials, quantified using the dimensionless Figure-of-Merit, ZT (= $TS^2/\rho\kappa$, where S, T, ρ, and κ are Seebeck coefficient, absolute temperature, electrical resistivity, and thermal conductivity, respectively) [1]. Nowadays, high ZT intermetallic materials [2,3] are applied in various sectors, e.g. automobile industry, even if these materials show several drawbacks, as their low thermal stability which can produce their degradation at high temperatures. In 1997, the discovery of high TE performances in Na_xCoO_2 ceramic [4] focused great research efforts on CoO-based materials. As a consequence, many works have led to raise TE performances of different members of the CoO-based family, such as $[Ca_2CoO_3][CoO_2]_{1.62}$, $[Bi_{0.87}AEO_2]_2[CoO_2]_{b1/b2}$ (AE: Alkaline earth) [5-8]. Detailed structural studies of these materials have shown that the crystal structure can be described using a monoclinic structure composed, in turn, by two different layers alternatively stacked. These two layers are a conductive CdI_2-type CoO_2 with a two-dimensional triangular lattice, and an insulating rock salt type (RS) block one. The two sublattices possess common *a*- and *c*-axis lattice parameters and β angles but different *b*-axis length, producing a misfit along the *b*-direction [9]. This structural anisotropy is reflected in a high electrical one, which makes necessary the alignment of the plate-like grains when looking for bulk properties close to the obtained on single crystals. Many processing methods have demonstrated their suitability to produce good grain orientation in different ceramic oxides. Among all these successful techniques, it is worth to mention the spark plasma sintering [10], template grain growth [11], directional growth from the melt [12], or the electrically assisted laser floating zone method (EALFZ) [13]. The materials produced through these techniques possess well oriented grains, reflected in the decrease of electrical resistivity when measured along the texturing direction (parallel to the *ab* plane of grains). On the other hand, it has been found that Pb doping in melt-textured Bi-AE-Co-O system (AE: Alkaline earth) leads to a reduction of electrical resistivity due to the raise of the Co oxidation state in the conducting layer by increasing the carrier concentration [14,15]. Moreover, it has been reported that metallic Ag addition enhances

electrical grains connectivity, decreasing electrical resistivity, without modifying the thermoelectric phase composition [16-18].

Taking into account the effects produced by texturing, Pb doping and Ag addition in the CoO-based materials, the aim of the present work is studying the evolution of microstructure and TE performances of optimally Pb doped [15] $Bi_2Ba_2Co_2O_y$ ceramics with the adequate Ag addition [19] when they are melt-grown at a relatively high rates. Moreover, as it is well known, these materials show incongruent melting leading to a mixture of different phases after solidification [20]. As a consequence, some of the samples will be annealed in order to decrease the amount of secondary phases, and their microstructural and electrical properties will be compared with the ones obtained in the as-grown samples, used as reference.

Experimental procedure

$Bi_{1.6}Pb_{0.4}Ba_2Co_2O_y$ + 3 wt.% Ag polycrystalline ceramics were prepared using the sol-gel route via nitrates due to the inherent advantages of this method [21]. Commercial $Bi(NO_3)_3 \cdot 5H_2O$ (≥ 98 %, Aldrich), PbO (Aldrich, 99 %), $BaCO_3$ (Panreac, 99 + %), $Co(NO_3)_2 \cdot 6H_2O$ (98 %, Panreac), and metallic Ag (99 %, Aldrich) powders were used as starting materials. They were weighed in the appropriate proportions and dissolved in a mixture of distilled water and concentrated HNO_3 (analysis grade, Panreac). Citric acid (99.5 %, Panreac), and ethylene glycol (99 %, Panreac), were added to the pink solution in the adequate proportions. Heating at 110 ºC onto a hot plate has been performed to evaporate the solvent until the formation of a dry light pink gel [21]. Further heating at 350 ºC produces the gel decomposition through a self-combustion process, leading to very fine and soft brownish powders. These remaining powders were hand-ground and thermally treated twice, under air, at 700 and 750 ºC for about 12 hours with an intermediate hand-milling to decompose the barium carbonate. The resulting black powders were then hand-milled, introduced into a latex rubber tube (inner diameter ~ 3 mm), and isostatically cold pressed at 200 MPa for one minute to obtain green ceramic cylinders (~ 100 mm long). These cylinders were subsequently used as feed in a laser floating zone (LFZ) device equipped with a continuous power Nd:YAG laser (λ = 1.06 μm) described elsewhere [22]. All the samples were processed at 30 mm/h under air, with a seed rotation of 3 rpm anticlockwise while the feed was rotated at 15 rpm, in the opposite direction, in order to assure the compositional homogeneity inside the molten zone. After the texturing process, long (~ 100 mm)

and geometrically homogeneous (~ 2 mm diameter) textured cylindrical rods have been produced. Finally, these bars were cut into pieces with the adequate dimensions for their TE characterization (~ 15 mm long pieces). Some of these samples were kept in the as-grown state to be used as reference, while some others were annealed under air at 750 ºC for 24 h, with a 3 ºC/min heating rate, followed by a final furnace cooling.

Structural characterization has been performed through powder XRD using a using a Rigaku D/max-B X-ray powder diffractometer (Cu Kα radiation) with 2θ ranging between 10 and 70 degrees. Microstructural evolution has been observed using a field emission scanning electron microscope (FESEM, Carl Zeiss Merlin) equipped with an energy X-ray dispersive spectroscopy (EDS) system. Longitudinal polished sections of as-grown and annealed textured samples have been observed using backscattered electrons to evaluate the phases composition. Electrical resistivity and Seebeck coefficient have been simultaneously determined by the standard dc four-probe technique in a LSR3 measurement system (Linseis GmbH) under He atmosphere, in the steady state mode, at temperatures ranging from 50 to 650 ºC. Samples performances have been determined through the power factor ($PF = S^2/\rho$), calculated from the previously measured electrical resistivity and Seebeck coefficient data.

Results and Discussion

Powder XRD data of as-grown and annealed $Bi_{1.6}Pb_{0.4}Ba_2Co_2O_y$ + 3 wt.% Ag textured materials are displayed in Figs. 1a and b, respectively. Both of them show very similar patterns and the most intense peaks (indicated by their diffraction planes) correspond to the misfit cobaltite $Bi_{1.6}Pb_{0.4}Ba_2Co_2O_y$ phase, in agreement with previously reported data [23,24]. Moreover, the small peaks appearing at around 30 and 38 degrees have been associated to a Bi(Pb)-Co-O solid solution with P4mm space group [25], and metallic Ag, respectively [26]. In spite of the typical incongruent melting of these materials, no clear differences between as-grown and annealed samples can be observed. This fact is due to modifications in the solidification conditions induced by Pb, which promotes the thermoelectric phase formation at higher rates than in Pb-free samples, as observed in related systems prepared through the same technique [14,27]. As a consequence, from these XRD results it seems that the annealing procedure has not produced drastic modifications in the phases proportions in these samples. Additionally, it can be deduced

that Ag has not reacted with the $Bi_{1.6}Pb_{0.4}Ba_2Co_2O_y$ ceramic in the as-grown or annealed samples [21].

The microstructural features observed in the as-grown and annealed $Bi_{1.6}Pb_{0.4}Ba_2Co_2O_y$ + 3 wt.% Ag textured materials are illustrated in Fig. 2. In the micrographs, four contrasts can be easily identified in both types of samples. EDS analysis has associated each contrast to a different phase. Grey contrast (#1) corresponds to the $Bi_{1.6}Pb_{0.4}Ba_2Co_2O_y$ phase, appearing as the major one in agreement with the XRD data. Dark and light grey ones (#2, and #3, respectively), have been associated to $Bi_5Co_5O_{14}$, and $Bi_{1.6}Pb_{0.4}BaO_3$ secondary phases, respectively, while #4 (grey contrast) is metallic Ag which can be only identified by its shape. As it can be observed when comparing both micrographs in the figure, annealing procedure decreases the amount of secondary phases and the cracks appearing between different composition grains. This effect is due to the cations diffusion promoted by the relatively high temperature reached in the annealing procedure, leading to the equilibrium phase formation and the associated grain growth which helps to heal the cracks.

The electrical resistivity of as-grown and annealed $Bi_{1.6}Pb_{0.4}Ba_2Co_2O_y$ + 3 wt.% Ag textured materials as a function of temperature is shown in Fig. 3. In the graph, it can be seen that both samples possess the same trend in the whole measured temperature range. They exhibit metallic-like behavior ($\delta\rho/\delta T < 0$) between room temperature and 200 ºC, and semiconducting-like one ($\delta\rho/\delta T > 0$) at higher temperatures. Moreover, the electrical resistivity values are clearly decreased after the annealing procedure, in agreement with the SEM observations and previously reported data which showed that LFZ procedure leads to materials with very high amount of oxygen vacancies [12] which could be at least partially filled during annealing [20]. The decrease of oxygen vacancies increases the carrier concentration, while the microstructural modifications improve the electrical grains connectivity. Both factors would contribute to lower electrical resistivity values than the obtained in the as-grown materials. In any case, it is important to highlight that the lowest resistivity value obtained for the annealed samples at room temperature, ~ 5.8 mΩ.cm, is much lower than the best reported for sintered $Bi_2Ba_2Co_2O_\delta$ materials (pure or Ag-doped), typically between 550 and 21 mΩ.cm [23,28-30]. Moreover, it is also lower than the best reported values in textured $Bi_2Ba_2Co_2O_\delta$ materials, between 10-250 mΩ.cm [8,12,15,31], and very close to the values reported in single crystals (4 mΩ.cm) measured along the ab plane [32,33]. When considering the high temperature values (650 ºC),

the minimum has been measured in the annealed samples (5.9 mΩ.cm), which is much lower than the ones found in sintered and textured $Bi_2Ba_2Co_2O_\delta$ materials (33 [28,30], and 8.5-50 mΩ.cm [8,12,15], respectively).

The Seebeck coefficient variation of as-grown and annealed $Bi_{1.6}Pb_{0.4}Ba_2Co_2O_y$ + 3 wt.% Ag textured materials, as a function of temperature, is displayed in Fig. 4. At a first sight it can be clearly seen that the Seebeck coefficient values are positive in the whole measured temperature range, indicating a conduction mechanism predominantly governed by holes. Moreover, S values increase when temperature is raised which can be associated with a metal or degenerated semiconductor typical behaviour when the variation of carrier concentration, effective mass, and Fermi level with temperature are negligible. At room temperature, both types of samples possess the same S values (112 μV/K), clearly indicating that oxygen diffusion has been negligible during the annealing procedure, due to the high density of samples, and relatively short time. This fact is confirming that the decrease on the electrical resistivity after annealing is only due to the improvement in the microstructure and no changes on the carrier concentration have been produced, when taking into account Koshibae's expression [34]. These maximum S values at room temperature are higher than the obtained in sintered materials (between 80 and 100 μV/K) [23,28-30], Ag doped samples (105 μV/K) [29], and comparable to the reported in single crystals (95-110 μV/K) [32,33]. On the other hand, they are lower than the measured in textured materials (115-145 μV/K) [8,12,15,31]. When comparing the high temperature values, the as-grown samples possess around 10 % higher S values at 650 ºC than the annealed ones. The maximum value at this temperature (177 μV/K) is higher than the reported for sintered materials (105-120 μV/K) [28,30,35], and are around the determined values in textured materials (145-185 μV/K) [8,12,15].

Thermoelectric performances of both kinds of samples were evaluated through their power factor presented, as a function of temperature, in Fig. 5. In the graph, it can be easily observed that as-grown and annealed samples follow a parallel trend with temperature. PF values are higher for the annealed samples in the whole measured temperature range, mainly due to the decrease of electrical resistivity. Furthermore, PF is nearly linearly increased when the temperature is raised in both types of samples. The maximum PF value at room temperature, 0.22 mW/K^2m, is much higher than the reported in sintered pure or Ag-doped materials (between 0.001 and 0.035

mW/K^{2}m) [23,28-31,35,36], textured (0.010-0.15 mW/K^{2}m) [8,12,15,31], and around to the best reported values for single crystals (0.2-0.3 mW/K^{2}m) [32,33]. At high temperatures (650 ºC), PF is drastically increased, reaching 0.46 mW/K^{2}m in the annealed samples, which is much higher than the obtained in sintered materials (0.013-0.040 mW/K^{2}m) [28,30,35], or than the best reported in laser textured materials grown at similar or even at very low rates (0.04-0.40 mW/K^{2}m) [8,12,15]. These very high PF values can be explained taking into account the good grain alignment, high density, low amount of secondary phases and cracks, and good electrical connectivity of grains in these bulk materials.

The maximum PF value obtained in this work is the highest one reported in the Bi-Ba-Co-O family in polycrystalline bulk materials so far in the best of our knowledge, making the annealed $Bi_{1.6}Pb_{0.4}Ba_2Co_2O_y$ + 3 wt.% Ag textured materials very good candidates to be applied in practical thermoelectric devices.

Conclusions

This work demonstrates that $Bi_{1.6}Pb_{0.4}Ba_2Co_2O_y$ + 3 wt.% Ag materials can be successfully textured using the LFZ technique. In spite of their relatively high amount of secondary phases and cracks, as-grown materials possess high thermoelectric performances. Annealing has been found to be very useful to increase the amount of thermoelectric phase and healing the cracks, promoting an enhancement of the electrical grains connectivity. These modifications are reflected in a drastic decrease of electrical resistivity, when compared with the measured in the as-grown materials. Oxygen diffusion has been discarded as one of the factors decreasing electrical resistivity due to the very similar room temperature Seebeck coefficient, in agreement with Koshibae's model. The highest power factor values at room temperature are around the reported ones for single crystals, while at 650 ºC they are the highest reported values in the Bi-Ba-Co-O family, in the best of our knowledge, approaching these materials to their practical applications.

Compliance with Ethical Standards:

Funding: This research has been supported by the MINECO-FEDER (Project MAT2013-46505-C3-1-R). The authors wish to thank the Gobierno de Aragón-FEDER (Consolidated Research

Groups T87 and T12) for financial support. Authors acknowledge the use of Servicio General de Apoyo a la Investigación-SAI, Universidad de Zaragoza.

Conflict of Interest: The authors declare that they have no conflict of interest.

References

1. Rowe D M (2006) Thermoelectrics handbook: macro to nano. CRC Press, Boca Raton

2. Wang H, Hwang J, Snedaker M L, Kim I H, Kang C, Kim J, Stucky G D, Bowers J, Kim W (2015) High Thermoelectric Performance of a Heterogeneous PbTe Nanocomposite. Chem Mater 27:944-949. doi: 10.1021/cm5042138

3. Santamaria J A, Alkorta J, Sevillano J G (2015) Microcompression Tests of Single-Crystalline and Ultrafine Grain Bi_2Te_3 Thermoelectric Material. J Mater Res 30:2593-2604. doi: 10.1557/jmr.2015.170

4. Terasaki I, Sasago Y, Uchinokura K (1997) Large Thermoelectric Power in $NaCo_2O_4$ Single Crystals. Phys Rev B 56:12685-12687. doi: 10.1103/PhysRevB.56.R12685

5. Funahashi R, Matsubara I, Ikuta H, Takeuchi T, Mizutani U, Sodeoka S (2000) An Oxide Single Crystal with High Thermoelectric Performance in Air. Jpn J Appl Phys 39:L1127-L1129. doi: 10.1143/JJAP.39.L1127

6. Constantinescu G, Rasekh Sh, Torres M A, Diez J C, Madre M A, Sotelo A (2013) Effect of Sr Substitution for Ca on the $Ca_3Co_4O_9$ Thermoelectric Properties. J Alloys Compds 577:511-515. doi: 10.1016/j.jallcom.2013.07.005

7. Maignan A, Pelloquin D, Hebert S, Klein Y, Hervieu M (2006) Thermoelectric Power in Misfit Cobaltites Ceramics: Optimization by Chemical Substitutions. Bol Soc Esp Ceram V 45:122-125.

8. Constantinescu G, Rasekh Sh, Torres M A, Madre M A, Diez J C, Sotelo A (2013) Enhancement of the High-Temperature Thermoelectric Performance of $Bi_2Ba_2Co_2O_x$ Ceramics. Scripta Mater 68:75-78. doi: 10.1016/j.scriptamat.2012.09.014

9. Itahara H, Xia C, Sugiyama J, Tani T (2004) Fabrication of Textured Thermoelectric Layered Cobaltites with Various Rock Salt-Type Layers by Using Beta-$Co(OH)_2$ Platelets as Reactive Templates. J Mater Chem 14:61-66. doi: 10.1039/b309804d

10. Noudem J G, Kenfaui D, Chateigner D, Gomina M (2011) Granular and Lamellar Thermoelectric Oxides Consolidated by Spark Plasma Sintering. J Electron Mater 40:1100-1106. doi: 10.1007/s11664-011-1550-z

11. Masuda Y, Nagahama D, Itahara H, Tani T, Seo W S, Koumoto K (2003) Thermoelectric Performance of Bi- and Na-Substituted $Ca_3Co_4O_9$ Improved through Ceramic Texturing. J Mater Chem 13:1094-1099. doi: 10.1039/b301758n

12. Rasekh Sh, Constantinescu G, Torres M A, Madre M A, Diez J C, Sotelo A (2012) Growth Rate Effect on Microstructure and Thermoelectric Properties of Melt Grown $Bi_2Ba_2Co_2O_x$ Textured Ceramics. Adv Appl Ceram 111:490-494. doi: 10.1179/1743676112Y.0000000039
13. Costa F M, Ferreira N M, Rasekh Sh, Fernandes A J S, Torres M A, Madre M A, Diez J C, Sotelo A (2015) Very Large Superconducting Currents Induced by Growth Tailoring. Cryst Growth Des 15:2094-2101. doi: 10.1021/cg5015972
14. Madre M A, Torres M A, Rasekh Sh, Diez J C, Sotelo A (2012) Improvement of Thermoelectric Performances of $Bi_2Sr_2Co_{1.8}O_x$ Textured Materials by Pb Addition Using a Polymer Solution Method. Mater Lett 76:5-7. doi: 10.1016/j.matlet.2012.02.026
15. Madre M A, Costa F M, Ferreira N M, Costa S I R, Rasekh Sh, Torres M A, Diez J C, Amaral V S, Amaral J S, Sotelo A (2016) High Thermoelectric Performance in $Bi_{2-x}Pb_xBa_2Co_2O_y$ Promoted by Directional Growth and Annealing. J Eur Ceram Soc 36:67-74. doi: 10.1016/j.jeurceramsoc.2015.09.034
16. Xiang P-H, Kinemuchi Y, Kaga H, Watari K (2008) Fabrication and Thermoelectric Properties of $Ca_3Co_4O_9$/Ag Composites. J Alloys Compds 454:364-369. doi: 10.1016/j.jallcom.2006.12.102
17. Wang S, Bai Z, Wang H, Lu Q, Wang J, Fu G (2013) High Temperature Thermoelectric Properties of $Bi_2Sr_2Co_2O_y$/Ag Composites. J Alloys Compds 554:254-257. doi: 10.1016/j.jallcom.2012.11.107
18. Sotelo A, Rasekh Sh, Constantinescu G, Torres M A, Madre M A, Diez J C (2013) Improvement of Textured $Bi_{1.6}Pb_{0.4}Sr_2Co_{1.8}O_x$ Thermoelectric Performances by Metallic Ag Additions. Ceram Int 39:1597-1602. doi: 10.1016/j.ceramint.2012.07.112
19. Rasekh Sh, Sotelo A, Torres M A, Bosque P, Madre M A, Diez J C (2016) Thermoelectric Properties of Directionally Grown $Bi_2Ba_2Co_2O_\delta$/Ag Composites: Effect of Annealing. J Mater Sci: Mater Electron. doi:10.1007/s10854-016-5435-z
20. Sotelo A, Torres M A, Constantinescu G, Rasekh Sh, Diez J C, Madre M A (2012) Effect of Ag Addition on the Mechanical and Thermoelectric Performances of Annealed $Bi_2Sr_2Co_{1.8}O_x$ Textured Ceramics. J Eur Ceram Soc 32:3745-3751. doi: 10.1016/j.jeurceramsoc.2012.05.035
21. Flahaut D, Allouche J, Sotelo A, Rasekh Sh, Torres M A, Madre M A, Diez J C (2016) Role of Ag in Textured-Annealed $Bi_2Ca_2Co_{1.7}O_x$ Thermoelectric Ceramic. Acta Mater 102:273-283. doi: 10.1016/j.actamat.2015.09.036

22. Angurel L A, Diez J C, de la Fuente G F, Gimeno F, Lera F, Lopez-Gascon C, Martinez E, Mora M, Navarro R, Sotelo A, Andres N, Recuero S, Arroyo M P (2006) Laser Technologies Applied to the Fabrication and Characterization of Bulk Bi-2212 Superconducting Materials for Power Application. Phys Status Solidi A 203:2931-2937. doi: 10.1002/pssa.200667005
23. Sakai K, Motohashi T, Karppinen M, Yamauchi H (2005) Enhancement in Thermoelectric Characteristics of the Misfit-Layered Cobalt Oxide, $[(Bi,Pb)_2Ba_{1.8}Co_{0.2}O_{4+/-\omega}]_{0.5}CoO_2$, Through Pb-for-Bi Substitution. Thin Solid Films 486:58-62. doi: 10.1016/j.tsf.2004.10.064
24. Sotelo A, Rasekh Sh, Torres M A, Bosque P, Madre M A, Diez J C (2016) Improved Thermoelectric Performances in Textured $Bi_{1.6}Pb_{0.4}Ba_2Co_2O_y$/Ag Composites. Ceram Int. doi: 10.1016/j.ceramint.2016.08.202.
25. Oka K, Azuma M, Chen W, Yusa H, Belik A A, Takayama Muromachi E, Mizumaki M, Ishimatsu N, Hiraoka N, Tsujimoto M, Tucker M G, Attfield J P, Shimakawa Y (2010) Pressure-induced spin-state transition in $BiCoO_3$. J Amer Chem Soc 132:9438-9443. doi: 10.1021/ja102987d
26. Becherer G, Ifland R (1954) Über eine präzisionsbestimmung der gitterkonstanten von silber nach dem rückstrahlverfahren. Naturwissenschaften 41:471-471.
27. Rasekh Sh, Madre M A, Diez J C, Guilmeau E, Marinel S, Sotelo A (2010) Effect of Pb Substitution on the Thermoelectrical Properties of Textured $Bi_2Ca_2Co_{1.7}O_y$ Ceramics Prepared by a Polymer Solution Method. Bol Soc Esp Ceram V 49:371-376.
28. Hao H, Yang H, Liu Y, Hu X (2011) High-temperature Thermoelectric Properties of Cu-substituted $Bi_2Ba_2Co_{2-x}Cu_xO_y$ Oxides. J Mater Sci Technol 27:525-528. doi: 10.1016/S1005-0302(11)60102-3
29. Ang R, Sun Y P, Luo X, Song W H (2007) A Narrow Band Contribution with Anderson Localization in Ag-Doped Layered Cobaltites $Bi_2Ba_3Co_2O_y$. J Appl Phys 102:073721. doi: 10.1063/1.2795622
30. Hao H, Yu H, Zhao L. (2011) Thermoelectric Characteristics of Pb- and La-Doped $Bi_2Ba_2Co_2O_y$ Ceramics. Adv Mater Res 228-229:804-808. doi: 10.4028/www.scientific.net/AMR.226-228.804
31. Motohashi T, Nonaka Y, Sakai K, Karppinen M, Yamauchi H (2008) Fabrication and Thermoelectric Characteristics of $[(Bi,Pb)_2Ba_2O_{4+/-\omega}]_{0.5}CoO_2$ Bulks with Highly Aligned Grain Structure. J Appl Phys 103:033705. doi: 10.1063/1.2838161

32. Kobayashi W, Hebert S, Muguerra H, Grebille D, Pelloquin D, Maignan A (2008) Thermoelectric Properties in the Misfit-Layered-Cobalt Oxides $[Bi_2A_2O_4][CoO_2]_{b1/b2}$ (A=Ca, Sr, Ba, b1/b2=1.65, 1.82, 1.98) Single Crystals. In: Prof. Kim I-H (ed) Proceedings ICT'07 IEEE, Piscataway, pp 117-120

33. Luo X G, Chen H, Wang G Y, Wu G, Wu T, Zhao L, Chen X H (2008) Transport Properties and Magnetic-Field-Induced Localization in the Misfit Cobaltite $[Bi_2Ba_{1.3}K_{0.6}Co_{0.1}O_4]^{RS}[CoO_2]_{1.97}$ Single Crystal. J Phys: Condens Matter 20:215221. doi: 10.1088/0953-8984/20/21/215221

34. Koshibae W, Tsutsui K, Maekawa S (2000) Thermopower in Cobalt Oxides. Phys Rev B 62:6869-6872. doi: 10.1103/PhysRevB.62.6869

35. Sakai K, Karppinen M, Chen J M, Liu R S, Sugihara S, Yamauchi H (2006) Pb-for-Bi Substitution for Enhancing Thermoelectric Characteristics of $[(Bi, Pb)_2Ba_2O_{4 +/-\omega}]_{0.5}CoO_2$. Appl Phys Lett 88:232102. doi: 10.1063/1.2206134

36. Hervieu M, Maignan A, Michel C, Hardy V, Creon N, Raveau B (2003) Metallicity and Thermopower of the Misfit Cobaltite $[Bi_2Ba_{1.8}Co_{0.2}O_4]^{RS}[CoO_2]_2$. Phys Rev B 67:045112. doi: 10.1103/PhysRevB.67.045112

Figure captions

Figure 1. Powder XRD patterns of $Bi_{1.6}Pb_{0.4}Ba_2Co_2O_y$/3 wt.% Ag samples textured at 30 mm/h: a) as-grown; and b) annealed. The diffraction planes indicated in the graph correspond to the $Bi_{1.6}Pb_{0.4}Ba_2Co_2O_y$ phase, while the peak marked with a + is associated to a Bi(Pb)-Co-O solid solution, and the one shown by #, to the (111) diffraction plane of metallic Ag.

Figure 2. SEM micrographs performed with backscattered electrons on longitudinal polished sections of $Bi_{1.6}Pb_{0.4}Ba_2Co_2O_y$/3 wt.% Ag samples textured at 30 mm/h: a) as-grown; and b) annealed. The numbers identified the different contrasts, associated through EDS to the phases: #1 (grey) $Bi_{1.6}Pb_{0.4}Ba_2Co_2O_y$; #2 (dark grey) Ba-Co-O solid solution; #3 (light grey) Bi-Pb-Ba-O solid solution; and #4 spherical metallic Ag particles.

Figure 3. Electrical resistivity evolution with temperature between room temperature and 650 ºC for as-grown and annealed $Bi_{1.6}Pb_{0.4}Ba_2Co_2O_y$/3 wt.% Ag samples textured at 30 mm/h.

Figure 4. Seebeck coefficient evolution with temperature between room temperature and 650 ºC for as-grown and annealed $Bi_{1.6}Pb_{0.4}Ba_2Co_2O_y$/3 wt.% Ag samples textured at 30 mm/h.

Figure 5. Power factor evolution with temperature between room temperature and 650 ºC for as-grown and annealed $Bi_{1.6}Pb_{0.4}Ba_2Co_2O_y$/3 wt.% Ag samples textured at 30 mm/h.

Figure 1

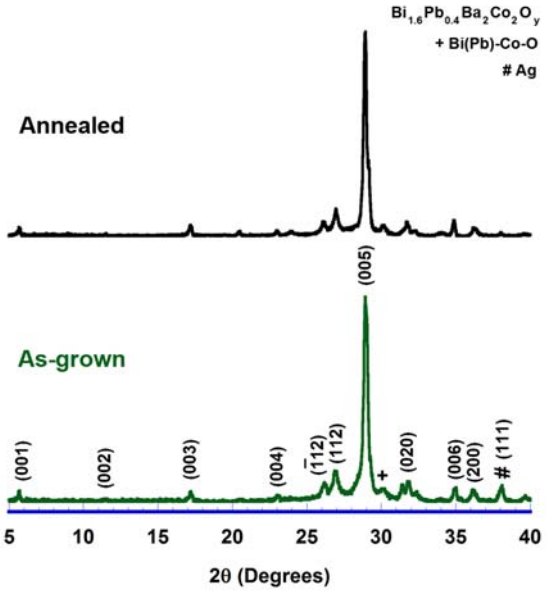
$Bi_{1.6}Pb_{0.4}Ba_2Co_2O_y$
+ Bi(Pb)-Co-O
# Ag
Annealed
As-grown
(001)
(002)
(003)
(004)
(112)
(112)
(005)
+
(020)
(006)
(200)
(111)
5
10
15
20
25
30
35
40
2θ (Degrees)

Figure 2

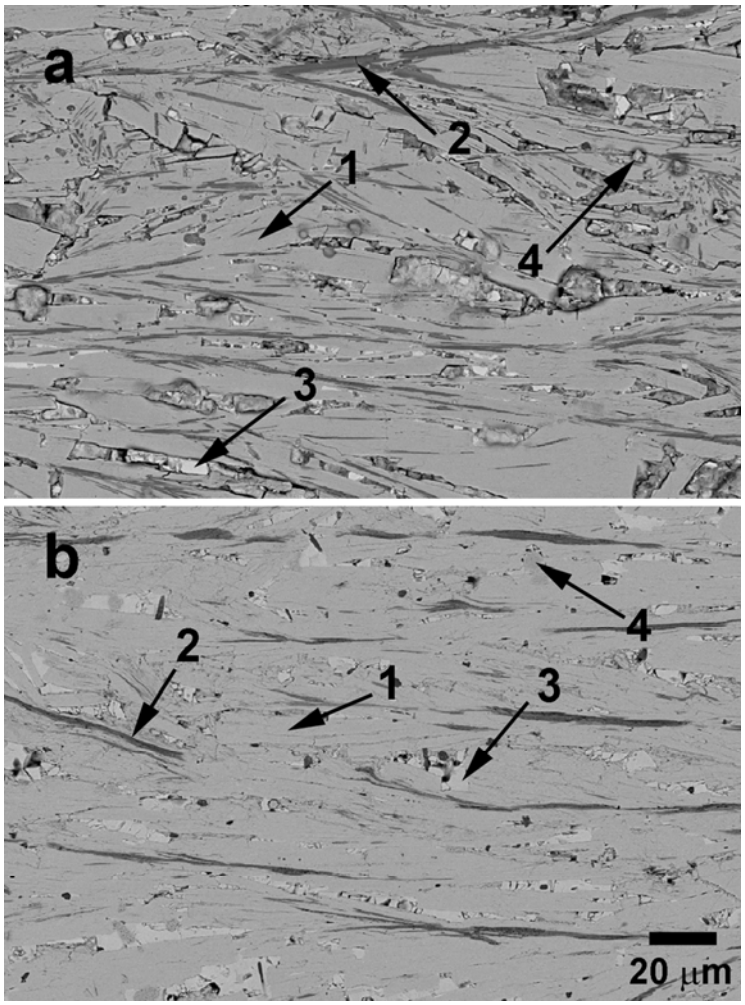

Figure 3

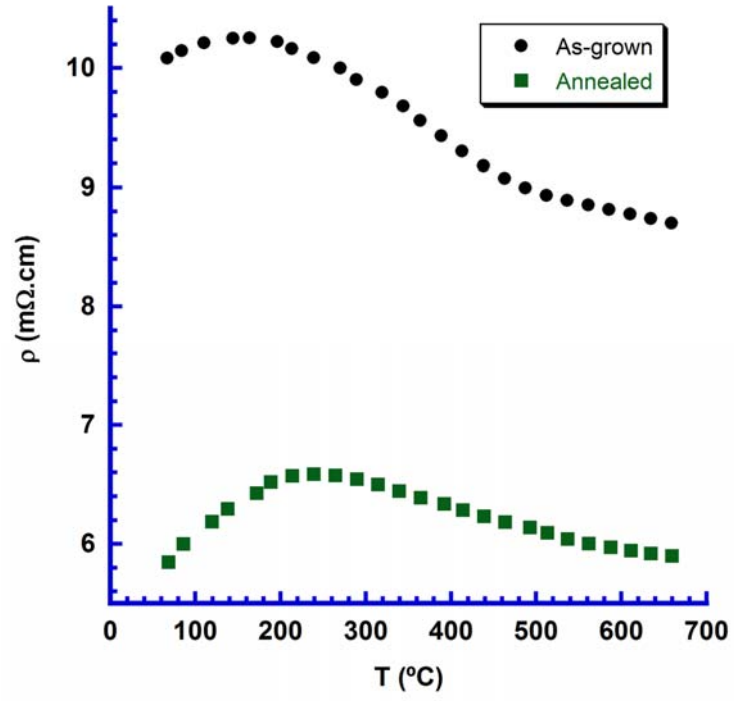
As-grown
Annealed
ρ (mΩ.cm)
10
9
8
7
6
0
100
200
300
400
500
600
700
T (°C)

Figure 4

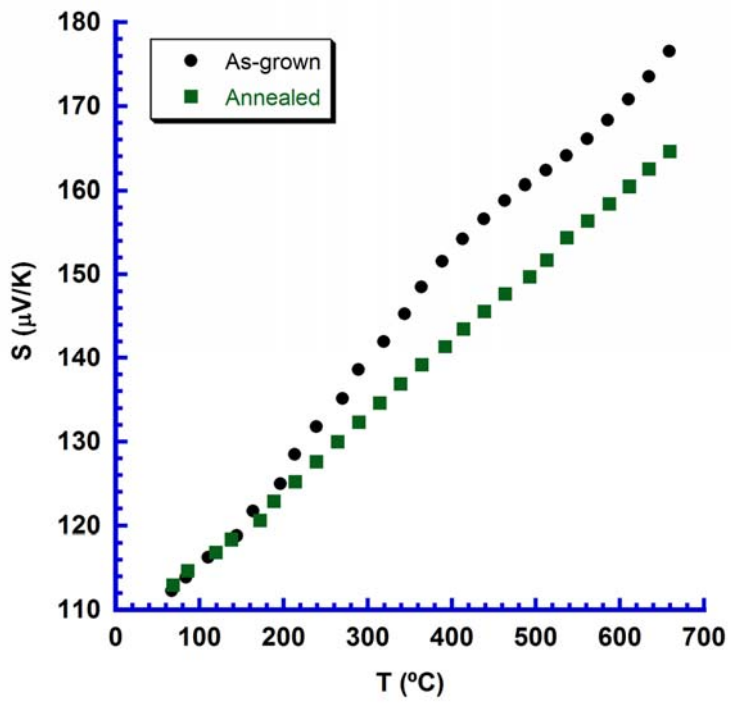
As-grown
Annealed
S (μV/K)
T (°C)
180
170
160
150
140
130
120
110
0
100
200
300
400
500
600
700

Figure 5

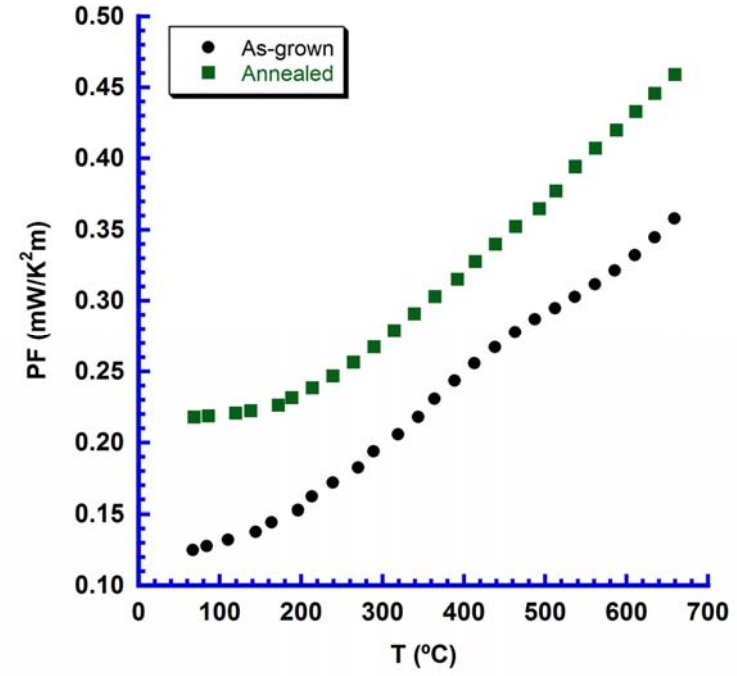
As-grown
Annealed
PF (mW/K²m)
T (°C)
0.50
0.45
0.40
0.35
0.30
0.25
0.20
0.15
0.10
0
100
200
300
400
500
600
700